Automatic sparse ESM scan using Gaussian process regression

Jiangshuai Li^{#1}, Jiahao Zhou^{#2}, Shaohui Yong^{#3}, Yuanzhuo Liu^{#4}, Victor Khilkevich^{#5}

EMC Laboratory, Missouri University of Science and Technology

Rolla, MO, USA

1 lijiangs, 2 jzqhx, 3 sy2m5, 4 liuyuanz, 5 khilkevichv@mst.edu

Abstract — Emission source microscopy (ESM) technique can be utilized for localization of electromagnetic interference sources in complex and large systems. In this work a Gaussian process regression (GPR) method is applied in real-time to select sampling points for the sparse ESM imaging using a motorized scanner. The Gaussian process regression is used to estimate the complex amplitude of the scanned field and its uncertainty allowing to select the most relevant areas for scanning. Compared with the randomly selected samples the proposed method allows to reduce the number of samples needed to achieve a certain dynamic range of the image, reducing the overall scanning time. Results for simulated and measured 1D scans are presented.

Keywords — ESM, Gaussian regression, Smart scanner, Emission ources, Location, Radiation strength.

I. INTRODUCTION

Emission source microscopy (ESM) is a technique that can localize and characterize radiation sources in complex systems by measuring the electromagnetic field magnitude and phase over the planar surface at a typical distance of several wavelengths away from the DUT [1].

Uniform ESM imaging provides the best results in terms of the image quality [2], but leads to a long scanning time needed to sample the fields on the plane with sub-wavelength step required to satisfy the Nyquist criterion [3]. To overcome the problem a sparse scanning strategy was proposed [4]. As [5] demonstrates, with the random selections of the sampling locations, the dynamic range of the image (related to the amount of noise added due to space sampling) is equal to the number of samples. And while sparse random sampling often produces satisfactory results, it still can lead to prohibitively long scanning times needed to achieve a desirable image quality. An alternative to random sampling is manual sampling [4], [6] which usually provides fast scanning but requires a human operation, and the scanning process is affected by operator's subjective decisions and perceptions. This paper proposes an automated method to select the sampling points based on the Gaussian process regression, eliminating a need of human intervention into the ESM process.

Gaussian process regression (GPR) can predict the field distribution based on randomly and sparsely measured samples. In this study, the Gaussian process regression is applied to select the next scanning location based on the previous ones. The automatic GPR ESM method can intelligently and automatically control the scanning process, reducing the number of

measurement points with less image quality degradation compared to the random ESM scanning.

The paper is organized as follows. Section II introduces the sparse ESM technique and Gaussian process regression. In Section III the system setup of sparse ESM using Gaussian process regression is illustrated, and the simulation and measurement results are demonstrated. Finally the summary is given.

II. INTRODUCTION OF SPARSE ESM AND GAUSSIAN PROCESS REGRESSION

A. Overview of Sparse ESM Technique.

The ESM algorithm is based on the synthetic aperture radar technique, which uses the two-dimensional (2-D) Fourier transformation. The field (image) on the DUT plane after backpropagation can be expressed as follows:

$$E_t^0(x, y, 0) = \mathcal{F}^{-1} \{ \mathcal{F}[E_t(x, y, z_0)] \cdot e^{jk_z z_0} \}, \tag{1}$$

where

$$\begin{aligned} k_z &= \sqrt{k^2 - k_x^2 - k_y^2}, & \text{if } k_x^2 + k_y^2 \le k^2, \\ k_z &= -j \sqrt{k^2 - k_x^2 - k_y^2}, & \text{otherwise.} \end{aligned}$$
 (2)

In (2) k is the wave number, and k_x, k_y, k_z are the components of the propagation vector (or the spatial frequencies in x-, y-, and z-directions). $E_t(x, y, z_0)$ is the tangential fields on the scanning planar surface (x, y) at the elevation z_0 above the image plane (see. Fig. 1).

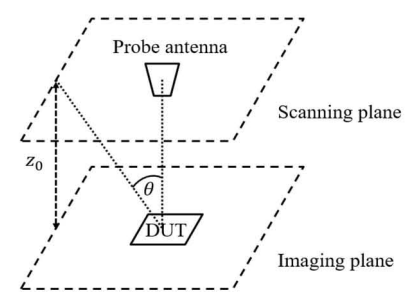


Fig. 1. 2-D ESM scanning arrangement.

Since the sparse ESM is carried out with non-uniform scanning points, a predefined grid of zero values is created before

the scanning and filled-in during the scanning process [2], [5]. The zero-valued grid should be defined with a step size much smaller than the wavelength to minimize the phase errors in the field caused by the difference of the actual and discretized locations of the probe. For example, when working at 3 GHz, the reasonable choice of the step could be 2 mm (12.5 points per wavelength), which could cause a relatively small phase as well as localization errors. At the same time the zeros in the scanned field distribution lead to noise in the image. The signal-to-noise ratio of the acquired image is approximately equal to the number of the sparse samples and does not depend on the density of the grid [5].

B. Introduction of Gaussian Process Regression.

A Gaussian process is a collection of random variables, any finite number of which have a joint Gaussian distribution [7]. A Gaussian process is completely specified by its mean value

$$\mu(w) = \mathbb{E}[(w)],\tag{3}$$

where w is the input vector (sampled function) and \mathbb{E} is the expected value operator, and a covariance function

$$k(w, w') = \mathbb{E}[(f(w) - \mu(w))(f(w') - \mu(w'))]. \tag{4}$$

Thus the Gaussian process can be written as

$$f(w) \sim GP(\mu(w), k(w, w')), \tag{5}$$

where f(w) is the estimated probability density of the process w, characterized by its mean value and covariance, and GP is the Gaussian process distribution.

Application of the GPR approximation is illustrated in Fig. 2. A certain function (the curve "Actual" in the figure) is sampled at several locations (marked by crosses). Application of the GPR allows to estimate the mean value of the function (" μ ") and its uncertainty (or the confidence interval " $\mu + \sigma$ " and " $\mu - \sigma$ ").

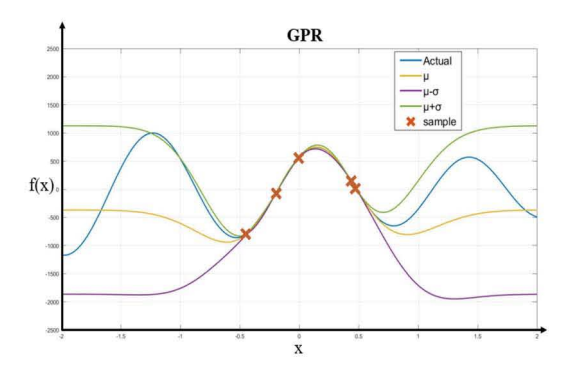


Fig. 2. An example of a 1D GPR estimation

The results of the GPR can be regarded as the fit of the function f(x) with the provided fit uncertainty. As can be seen from the example, the function f(x) is well fitted at the interval from approximately -0.5 to 0.5 (this interval is characterized by small predicted uncertainty), and it is reasonable to add the consecutive sampling points outside this interval where the predicted uncertainty is large.

To perform the GPR fit the Matlab implementation of the Gaussian process regression is used throughout the rest of the paper. The main parameter needed to perform the GPR is the minimum value of the standard deviation σ_{min} . This value is important because it allows to set the "size" of the features that are supposed to be fitted by the GPR. If the minimum sigma

value is too large, the function could be approximated by a constant (the variations of the function would be within the $\pm \sigma_{min}$ band relative to the constant). If the minimum value is too small, the GPR would try to fit measurement errors (such as additive noise), which is undesirable. The choice of the minimum value of sigma is an important problem, which requires additional investigation. In the presented implementation the minimum value of sigma was selected empirically.

C. Sparse ESM system using GPR

The GPR is performed separately for real and imaginary parts of the measured field distribution. As the result of the GPR, the mean values μ_{real} and μ_{imag} as well as the standard deviations σ_{real} and σ_{imag} are estimated (all of these quantities are functions of the spatial coordinates on the sampling plane or line). The total field power and its uncertainty are then calculated as

$$P = \mu_{real}^2 + \mu_{imag}^2 \,, \tag{6}$$

$$\sigma = \sqrt{\sigma_{real}^2 + \sigma_{imag}^2} \ . \tag{7}$$

Obviously the regions with the largest power on the scan plane contribute the most to the ESM image. At the same time the large uncertainty in estimated field distribution leads to the large uncertainty in the image. So it is reasonable to scan primarily at the regions with high estimated power and high uncertainty. To satisfy these two requirement and empirical criterion was developed. According to it the next measurement is performed at the location x_{n+1} (n being the number of previously acquired samples) with the maximum product of the predicted power and uncertainty. At the same time, the next measurement point should not be closer than a certain distance ε (typically a fraction of a wavelength) to already sampled ones x_i to avoid undesirable clustering effect (see [2] for details):

$$x_{n+1} = x | \max[\sigma \cdot P],$$

$$\forall i \in [1, n], |x_{n+1} - x_i| \ge \varepsilon.$$
 (8)

The GPR fit can be performed if at least two samples are available. In the proposed implementation the first two initial samples are taken at random locations. The complete flow diagram of the process is shown in Fig. 3.

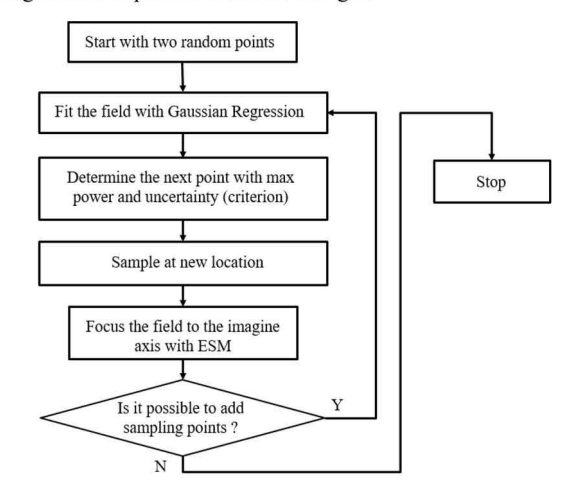


Fig. 3. Flow diagram of real-time automatic ESM using GPR

Because of the constrain in (8), the distance between the sampling points cannot be smaller than ε , which allows to have only a limited number of samples in the scanning area. This leads to the natural stop of the algorithm when no more sampling points can be added.

The ESM imaging can be performed periodically during the scan to observe image evolution in real time, or after the stop of the algorithm.

III. SIMULATION AND MEASURMENT REULTS

A. Simulation Result (1D).

In the simulation of the automatic sparse ESM using Gaussian process regression, three horizontally oriented dipoles are put on the image line at different positions. The working frequency is 10 GHz, with the wavelength λ =0.03 m, and the length of the scanning and image lines is 20 λ (0.6 m). The E_x (tangential) component of the field due to the dipoles was calculated on the scan line using analytical formulas for an infinitesimal dipole [8]. The parameters of the dipoles are listed in Table 1.

Table 1 Parameters of radiation sources used in simulation.

Source	Dipole 1	Dipole 2	Dipole 3	
Position	-8	1	5	
[λ]	0.01	1	1	_
Dipole moment [A·m]	0.01	I	1	

To verify the performance of the GPR method, the random sampling method is simulated as a comparison. The images obtained as the result of the ESM process are normalized to their corresponding maxima to facilitate their comparison (the absolute values of the images depend on the number of samples and the sampling step). Estimation of the absolute value of the image can be performed using interpolation of the scanned field as described in [4]. Accuracy of this process with respect to the GPR imaging requires additional investigation.

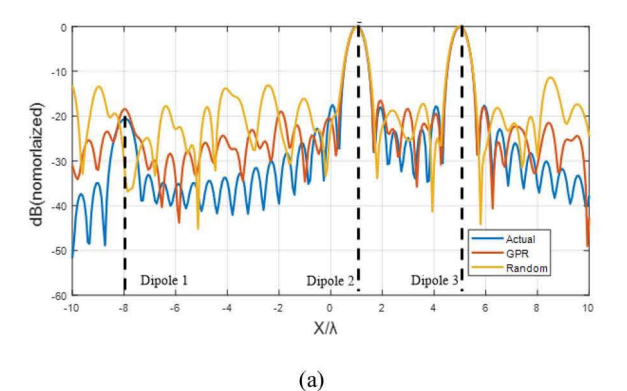
To quantify the error of the obtained image the mean squared difference between the normalized images is calculated:

$$MSE_E = \frac{1}{m} \sum_{i=1}^{m} \left(\frac{|E_S(i)|}{\max|E_S|} - \frac{|E_0(i)|}{\max|E_0|} \right)^2, \tag{9}$$

where E_S is the image obtained by using the GPR or the random sampling method, E_0 is the actual image (complete uniform scan), and m is the number of the samples in the image (i.e. the on the samples in the predefined grid).

The images obtained by taking 120 samples randomly or by the GPR selection with comparison to the actual image are show in Fig. 4 (a). As can be seen, even with this relatively low number of points the GPR sampling allows to resolve the weak source (dipole 1), while in the image obtained by the random sampling, the weak source cannot be identified because of high level of noise. The evolution of the mean squared error in the scanning process is illustrated by Fig. 4(b). As can be seen, the accuracy of the GPR imaging (characterized by the corresponding MSE value) is consistently better than that of the random sampling starting from approximately 70 acquired samples and after 120

iterations the error in the GPR imaging error is approximately 10 times lower than that of the random scanning process. Both plots in Fig. 4 demonstrate the advantage of the GPR imaging over random sampling in terms of the scanning time – i.e. the ability to obtain the image of better quality for the same number of acquired samples, or to reduce the number of samples needed to obtain an image of a certain quality.



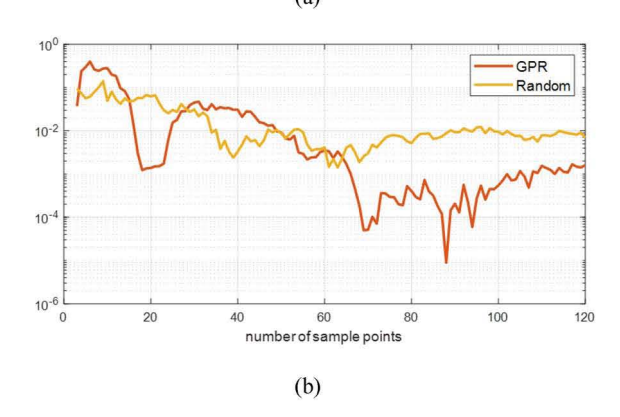


Fig. 4. Images obtained by GPR and random sampling: ESM image with 120 measured samples (a), the MSE_E as a function of the number of sampling points (b)

B. Measurement results (1D).

The scanning system setup is illustrated in Fig. 5. The scanning probe is attached to the carriage that can move on a frame. The carriage is moved by two stepper motors with two timing belts. The Microcontroller Unit (MCU) receives commands from the PC and controls the stepper motors.

The DUT on the image plane and the probe on the scanning plane are both log-periodic antennas with the working frequency range of 850-6500MHz. The antennas are connected to the VNA ports. By measuring the transmission coefficient (S_{21}) between the antennas it is possible to measure the complex values of the field amplitude at the scanning antenna location (scaled by the unknown, but irrelevant in this case, antenna and cable factors). The measured component is determined by the orientation of the scanning log-periodic antennas (x or y).

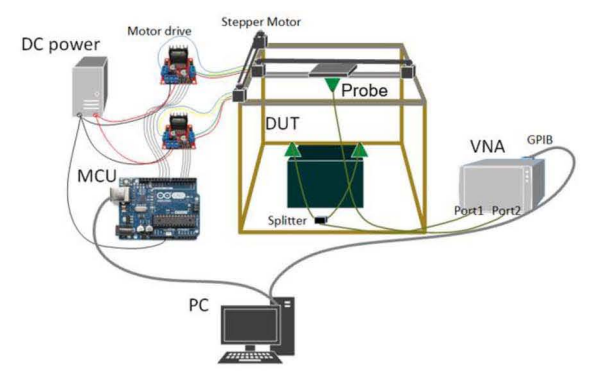


Fig. 5. Automatic sparse ESM system setup

The scanner allows to perform 2D scans, but only 1D scan results are reported in this paper. Implementation of the 2D scanning with the GPR is subject of the ongoing work.

In the 1D scans only one motor of the scanner is engaged and the scanning is performed along the line over the DUT (Fig. 6). In the scanning process the predefined zero-valued array is filled with the sampled field values. The extent of the scan range is 0.6 m with 6001 pre-defined sampling locations, resulting in the sampling step of 0.1 mm. The measurements are performed at 3 GHz.

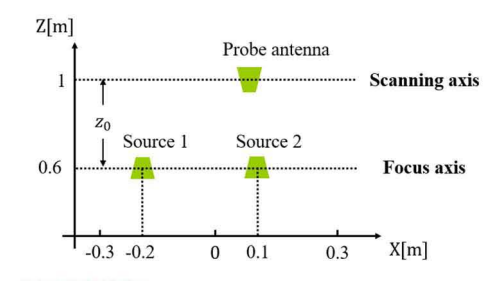


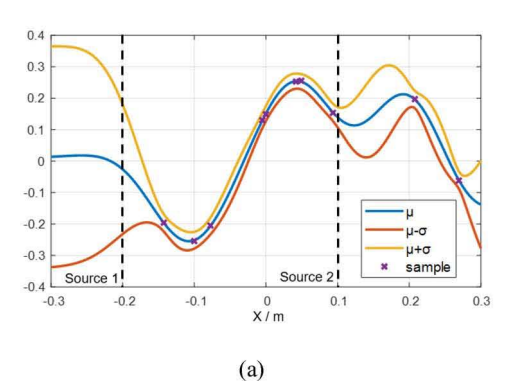


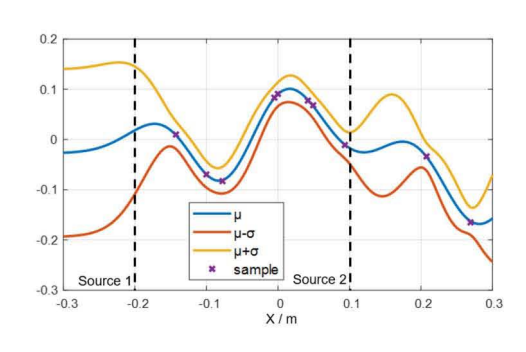
Fig. 6. Measurement setup geometry and photo.

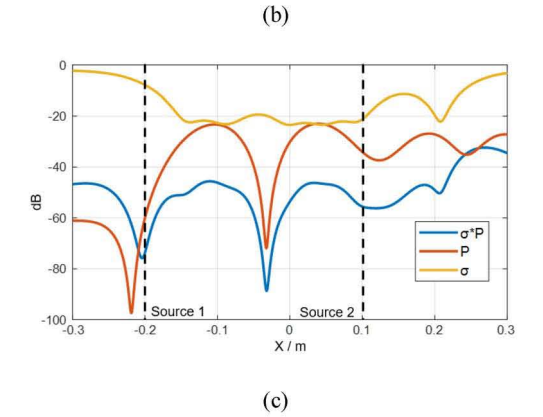
Fig. 6 illustrates the source arrangement. Two antennas are placed on the focus line at locations -0.2 m and 0.1 m (0 corresponds to the center of the scan line); the distance between the focus line and the scanning axis is 0.4 m. The two source antennas are connected to the VNA through a splitter, providing roughly equal excitation. By measuring the S_{21} between the VNA ports, the field on the scanning axis is obtained. Similar to the simulated results presented in the previous section, uniform, random, and GPR sampling measurement were performed. The total number of sampling points of the uniform sampling measurement was 241 (sampling step was 2.5 mm corresponding to 40 samples per wavelength.

Next two figures illustrate the convergence process during the GPR scan. Fig. 7 (a), (b) show the fit of the real and imaginary parts of the field after 10 acquired samples. As can be seen, the GPR instructed the scanner to scan primarily over source 2, where the field is already collected with relatively high density and accuracy. Fig. 7 (c) shows the curves related to the criterion (8), and Fig. 7 (d) demonstrated the image obtained after collecting 10 samples in comparison to the reference (result of the uniform scan). After 10 samples the images already start to reveal two peaks corresponding to two sources, and while the image quality is low in both GPR and random cases, the GPR image is already closer to the reference (uniform scan) than the random scan image.

Fig. 8 demonstrates the results at 100^{th} iteration (close to the end of the GPR scan process), showing convergence of the GPR and the random sampling images to the reference. As can be seen, the GPR sampling points cover the scan line almost uniformly; however, the samples are not collected around points x = -0.03 m, x = -0.18 m, and x = 0.13 m which correspond to the nulls of the field power, demonstrating intelligent scan point selection. After 100 sampling the image obtained by the GPR scanning is significantly better than that obtained by the random scan (Fig. 8 (d)).







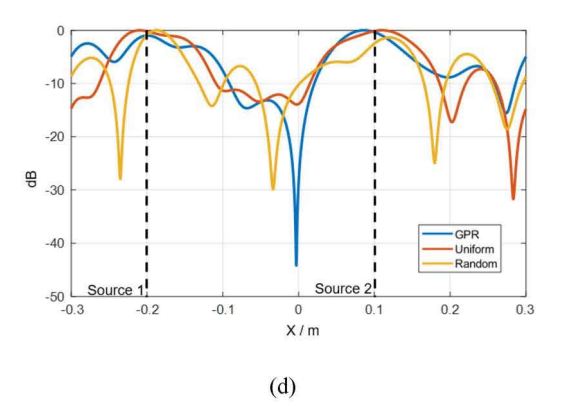
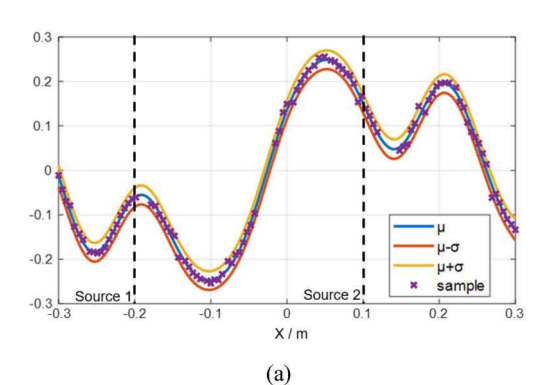
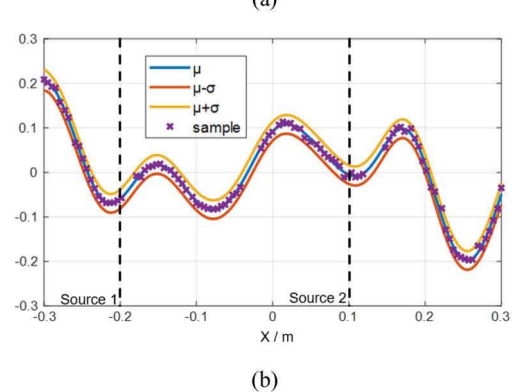
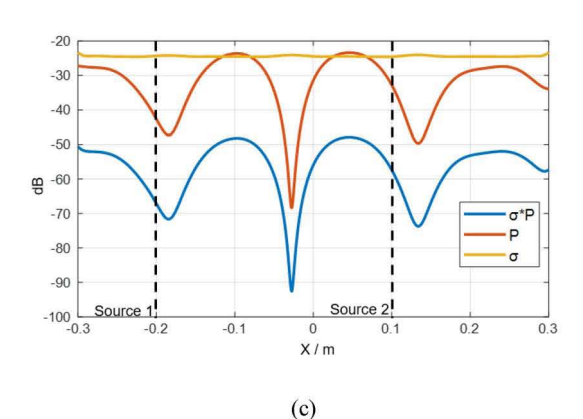


Fig. 7. GPR ESM scanned field and ESM image obtained after 10 samples: predicted real part (a), predicted imaginary part (b), predicted power and uncertainty (c), ESM images for GPR,uniform, and random scanning (d)







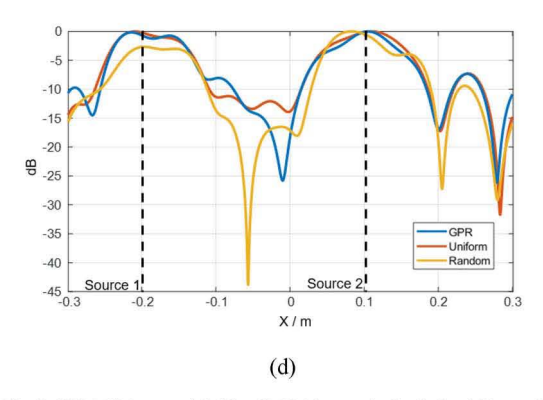


Fig. 8. GPR ESM scanned field and ESM image obtained after 100 samples: predicted real part (a), predicted imaginary part (b), predicted power and uncertainty (c), ESM images for GPR, uniform, and random scanning (d)

IV. SUMMARY

An automatic sparse ESM using Gaussian process regression method has been developed. Using the proposed method, the quality of the ESM imaging can be improved compared to the random scan without using operator-controlled setup. The number of the scan points can be potentially reduced compared to uniform and random scan due to intelligent selection of scan areas relevant for the image.

ACKNOWLEDGMENT

This material is based upon work supported by the National Science Foundation (NSF) under Grants IIP-1440110.

REFERENCES

- [1]. P. Maheshwari, H. Kajbaf, V. V. Khilkevich, and D. Pommerenke, "Emission source microscopy technique for EMI source localization," IEEE Trans. Electromagn. Compat., vol. 58, no. 3, pp. 729–737, Jun. 2016.
- [2]. M. Sørensen, H. Kajbaf, V. V. Khilkevich, L. Zhang and D. Pommerenke, "Analysis of the Effect on Image Quality of Different Scanning Point Selection Methods in Sparse ESM," in IEEE Transactions on Electromagnetic Compatibility, vol. 61, no. 6, pp. 1823-1831, Dec. 2019.
- [3].Y. Liu, J. Li, S. Yong, R. He and V. Khilkevich, "Scanning of random fields using blind source separation," 2019 IEEE International Symposium on Electromagnetic Compatibility, Signal & Power Integrity (EMC+SIPI), New Orleans, LA, USA, 2019, pp. 235-240.
- [4]. J. T. Case, M. T. Ghasr, and R. Zoughi, "Nonuniform manual scanning for rapid microwave nondestructive evaluation imaging," IEEE Trans. Instrum. Meas., vol. 62, no. 5, pp. 1250–1258, May 2013.
- [5]. L. Zhang, V. Khilkevich and D. Pommerenke, "Sparse Emission Source Microscopy for Rapid Emission Source Imaging," in *IEEE Transactions on Electromagnetic* Compatibility, vol. 59, no. 2, pp. 729-738, April 2017.
- [6]. H. He, V. Khilkevich and D. Pommerenke, "2D imaging system with optical tracking for EMI source localization," 2015 IEEE Symposium on Electromagnetic Compatibility and Signal Integrity, Santa Clara, CA, 2015, pp. 107-110.
- [7]. C. E. Rasmussen & C. K. I. Williams, Gaussian Processes for Machine Learning, the MIT Press, 2006, ISBN 026218253X. © 2006 Massachusetts Institute of Technology.
- [8]. C. A. Balanis, Antenna Theory: Analysis and Design, New York: Wiley, 1982.